Renewable Energy

Renewable Energy:

Selected Issues Volume II

Edited by

Manuel Pérez-Donsión, Silvano Vergura
and Gianpaolo Vitale

Cambridge
Scholars
Publishing

Renewable Energy: Selected Issues Volume II

Edited by Manuel Pérez-Donsión, Silvano Vergura and Gianpaolo Vitale

This book first published 2016

Cambridge Scholars Publishing

Lady Stephenson Library, Newcastle upon Tyne, NE6 2PA, UK

British Library Cataloguing in Publication Data
A catalogue record for this book is available from the British Library

ISBN (10): 1-4438-8524-X
ISBN (13): 978-1-4438-8524-9

As a two-volume set:
ISBN (10): 1-4438-8803-6
ISBN (13): 978-1-4438-8803-5

TABLE OF CONTENTS

Volume I

Part I: Data Management

Part II: Distributed Generation Issues

Volume II

Part VI: Solar Technologies

Part VIII: Wind and Marine Power Generation

PART VI:

SOLAR TECHNOLOGIES

CHAPTER THIRTY-TWO

MODELLING THE PRIMARY LOOP OF A CONCENTRATING SOLAR POWER PLANT

SILVANO VERGURA[1]

Abstract

A Matlab based model of the primary loop of a Concentrating Solar Power plant (CSP) is proposed. The modelled system considers the technology of parabolic troughs with a binary mixture of salts as the heat transfer fluid. The model is based on the layout of a pilot project to be implemented in the South of Italy, but it can be also used for different typologies of CSP, because it was implemented as a Graphical User Interface (GUI), which allows input data to be modified. As that project also contains thermal storage, the input and output temperatures are well defined. This choice removes the typical disadvantage of some renewable energy sources, i.e. the unpredictability of energy production. In this paper, only the primary loop of the whole system was modelled. The model permits the calculation of the main output variables of the primary loop: thermal performance, thermal power and thermal efficiency. The proposed model does not take into account transient phenomena and variable ambient conditions.

Keywords: CSP, Matlab model, molten salts, thermal efficiency, thermal power.

[1] Technical University of Bari, Dept. of Electrical and Information Engineering, st. E. Orabona 4, 70125 Bari, Italy. Email: silvano.vergura@poliba.it

Nomenclature

c_{ps}	Specific heat of the mixture of salts, J kg^{-1} K^{-1}
DNI	Direct Normal Irradiation, kWh m^{-2} day
GHI	Global horizontal Irradiation, kWh m^{-2} day
h_c	External convective heat transfer coefficient, W m^{-2} K^{-1}
h_d	Heat transfer coefficient for low-density gas, W m^{-2} K^{-1}
G_s	Flow capacity, kg/s
L, l	Length, m
Nu	Nusselt number
Pr	Prandtl number
$Q_{ab,r}$	Losses of the absorber for radiation, W
$Q_{ab,c}$	Losses of the absorber for conduction, W
Q_b	Losses due to the metal bellows, W
Q_{fluid}	Thermal power, W
$Q_{g,r}$	Losses of the glass for radiation, W
$Q_{g,c}$	Losses of the glass for convection, W
Q_{losses}	Total losses, W
r	Radius, m
Re	Reynolds number
S	Heated surface, m^2
T_g	Temperature, K
T_U	Thermal performance, K
ε_g	Emissivity of the glass, 0.9
ε_{ab}	Emissivity of the absorber
η	Thermal efficiency
λ	Thermal conductivity, W m^{-1} K^{-1}
ρ	Density, kg m^{-3}
σ	Stefan-Boltzmann constant, 5.67 *10^{-8} W m^{-2} K^{-4}

Introduction

The CO_2 emissions are considered responsible for the climate changes on Earth. As these emissions are also produced by burning fossil fuels to produce electrical energy, many countries in the world are transforming their national electrical production systems, decreasing the electrical production deriving from fossil fuels and increasing that deriving from Renewable Energy Sources (RES). Among RES, solar technologies are motivating a large interest. Moreover, the green paper of the Commission of the European Communities [1] reports that half of the gas consumption

in the EU came from only three countries (Russia, Norway, Algeria) and the oil and gas prices nearly doubled in the EU over the past two years, with electricity prices following. Therefore, the EU strategy for energy is to reach the target of 20% of energy produced by RES until 2020. This paper focuses on Concentrating Solar Power plants (CSP) because they are acquiring an increasing interest, especially if built with thermal energy storage [2]-[3]-[4]. Moreover, economic issues for the CSP have been treated in order to verify the profits, the breakeven point and so on [5]-[6].

Inorganic nitrate salt mixtures are often preferred as a fluid because they offer a favourable combination of density, specific heat, very low chemical reactivity, vapour pressure and cost ($0.40–$0.90/kg) [6]. The three main candidate salts include: a) Hitec, a ternary mixture of $NaNO_2$, $NaNO_3$ and KNO_3; b) Hitec-XL, a ternary mixture of $Ca(NO_3)_2$, $NaNO_3$, and KNO_3; c) a binary salt mixture of $NaNO_3$ and KNO_3. The latter salt has the lowest cost and the minimum inventory temperature is at least 80°C above the freezing point; therefore, it will be considered in this paper. Obviously, the heat transfer fluid must be chosen taking also into account the Operation and Maintenance (O&M) costs. A detailed analysis of the O&M costs related to a CSP fed by molten salts is reported in [7], where important issues are considered, such as: routine freeze protection, solar field preheat methods, collector loop maintenance and the selection of appropriate materials for piping and fittings.

The CSPs can be categorized into three main technologies, based on the process of collecting and concentrating solar radiation [8]: a) Parabolic Trough, b) Solar Tower for Central Receiver, c) Parabolic Dish. There is also a fourth technology (Linear Fresnel Reflector), but it is less common than the previous ones.

The first one uses parabolic trough shaped mirrors to concentrate the incident Direct Normal Irradiation (DNI) onto a receiver tube which is placed at the focal line of the trough. This is the most commercial technology for CSPs because it is the most mature technology. As this technology is considered in the paper, an in depth description is reported in the next section.

In the Solar Tower technology, the solar collector field contains a radial arrangement of several large sun tracking mirrors that concentrate the solar energy onto the receiver placed on the top of a central tower.

The third technology uses a parabolic dish-shaped solar concentrator that concentrates the sunlight onto a receiver placed at the focal point of the dish.

The paper is organized as follows: Section 3 presents a description of the CSP under test, Section 4 shows the Matlab based model and Section 5

discusses the results obtained by the Matlab-based GUI. Conclusions end the paper.

This chapter is the based on the revised version of the paper presented at the International Conference on Renewable Energies and Power Quality (ICREPQ'12) [9].

Description of the CSP under test

This paper focuses on the CSP based on parabolic troughs. An Italian pilot project named Archimede [10], based on this technology, was proposed by ENEL (Italy's largest power utility) and ENEA (Italian National agency for new technologies, energy and sustainable economic development) in the South of Italy.

The CSP model proposed in this paper utilized Archimede as a reference. Sub-section A presents the components, while sub-section B describes the layout of the proposed model.

Components and operation of the CSP

The CSP under investigation is constituted by the following main components:

- linear parabolic trough-shaped mirrors, named collectors, to focus the sun's rays onto a receiver pipe (inside and coaxial with a vacuum glass pipe) running along the focal line and containing a flowing fluid;
- hydraulic circuit with molten salts that connects the field of reflectors and the storage system, including the control system for controlling the temperature of the salts and the devices for loading and unloading the salts;
- pumping systems of the salts;
- storage system consisting of two tanks with a circular section;
- electrical power station equipped with two steam turbines (high and low pressure, respectively), a molten salt steam generator, a condenser with an appropriate cooling system (water or air) and the feed water preheating system.

The reflectors concentrate the sun's rays on the receiver and the heated fluid is transported to the energy conversion system. During this step, a part of the fluid can be stored for a posterior use. Then the remaining part is utilized to produce electrical energy. The energy conversion system is

similar to that of a common fossil fuel plant utilizing a thermal steam Rankine cycle. Usually, a mineral oil is used but it is expensive and highly flammable, and therefore can lead to important problems if it leaks at the operating temperature (290-390°C). For these reasons, a fluid constituted by a mixture of salts, sodium (60%) and potassium (40%) nitrate was considered; this fluid is largely used in the industry because it is chemically stable up to 600°C and causes no corrosion problems.

Moreover, the thermal storage system enables the storing of the solar energy, which can then be used when the sun is not present (during the night, in the presence of clouds and so on). This is a very important task for each solar plant. In fact, the unpredictability of energy production is the main disadvantage of solar plants, and is usually pointed out by the detractors of solar energy plants. Thermal storage enables decoupling thermal energy collecting from electrical energy production, i.e. it is not necessary to produce and to use the electrical energy just when the thermal energy is collected. In this way, it is possible to have a more efficient operation of the electrical generator, eliminating the stops due to cloudiness and making the system more compatible with the demands of the electricity grid. Fig. 1, from [10], reports a simplified scheme of the CSP. Three circuits are present:

1. the primary loop, devoted to the harvesting, distribution and storage of the solar thermal energy;
2. the secondary loop, where the thermal energy stored in the hot tank is utilized in the steam generator;
3. the thermal cycle, where thermal energy is transformed into electrical energy.

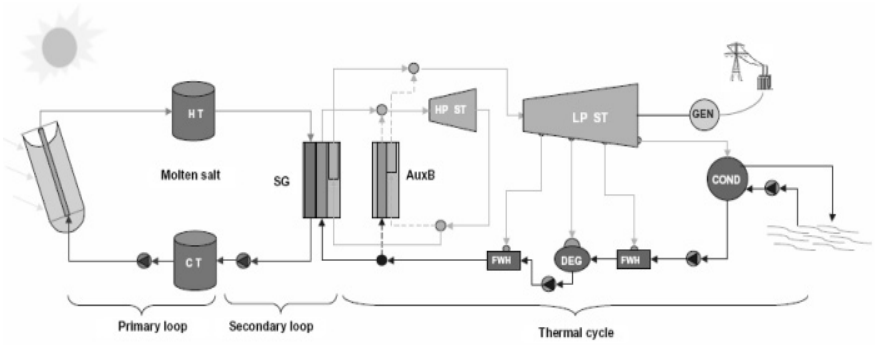

Fig. 1. CSP under investigation

The operation principle of the CSP under investigation is the following.

When direct solar radiation is present, the thermal fluid, taken from the cold tank at a temperature of 290°C, flows into the receivers and heats up until 550°C. Then, it is pumped into the hot tank, where it is stored. The flow of molten salts into the primary circuit is adjusted with respect to the solar radiation in order to maintain the input temperature of the hot tank constant. As the molten salts have a high temperature of solidification (238°C), it is necessary to maintain a minimum flow capacity when the solar radiation is not present or to provide heating systems of the pipes to avoid the fluid temperature falling below that point.

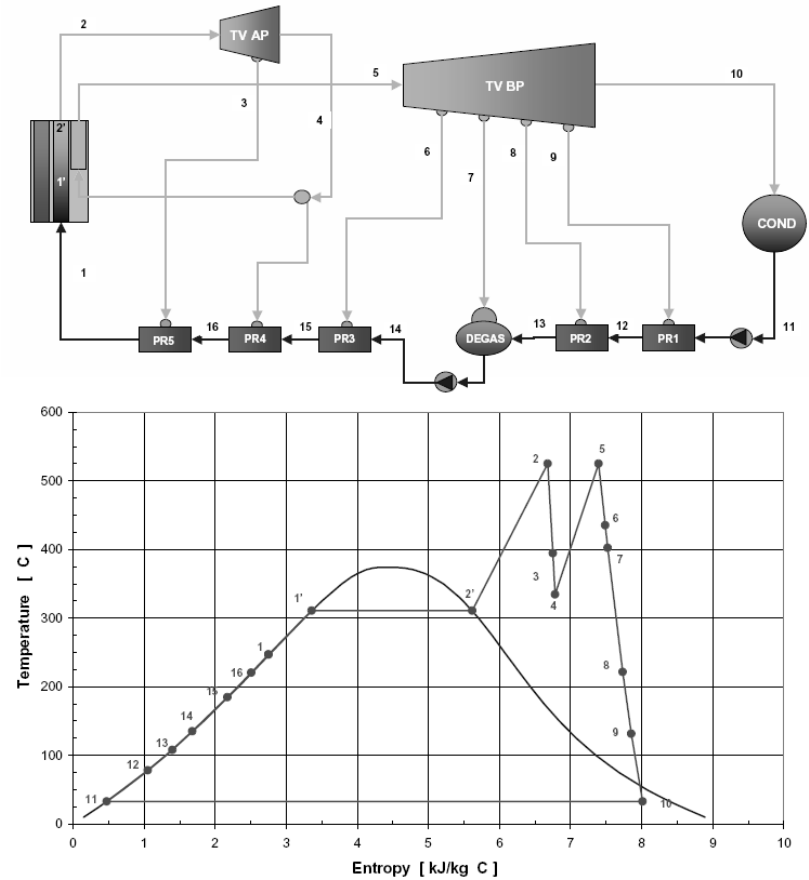

Fig. 2. Thermal cycle (a) and T-E diagram (b).

When electrical energy is requested, the salts stored in the hot tank are pumped into the heat exchanger, where steam at high pressure and temperature is produced. Then, the molten salts are collected in the cold tank. As already said, the thermal cycle is similar to that of a common fossil fuel power station. Two turbines for high and low pressure are present (Fig. 1); the superheated steam has a temperature of 525°C and a pressure of 120 bar when it expands through the high pressure turbine. The electrical rated power of the CSP is 40 MW, while the efficiency of the thermal cycle is equal to 42.3% in rated power conditions. A detailed representation of the thermal cycle is reported in Fig. 2a, while Fig. 2b represents the Temperature-Entropy diagram [10]. The numeration in the upper figure allows the path of the fluid to be followed, while the lower figure highlights the temperature value at each corresponding step.

Layout of the collectors and characteristic parameters

Fig. 3, from [10], reports the layout of the modelled CSP. It can be observed that the thermal power station (turbines, steam generator, condenser and tanks) is in a central position, while the solar field is constituted by three areas, two of them containing 33 Solar Collector Assembly (SCA) and third one containing 70 SCA. The SCA are parallel-connected to each other. Each SCA of each area is constituted by six series-connected collectors and each collector is 100m long and has a span of 5.76m. Therefore, one SCA is 600m long while the distance between two SCA is equal to 2 times the span of a collector. Table 1 reports the main parameters of the CSP.

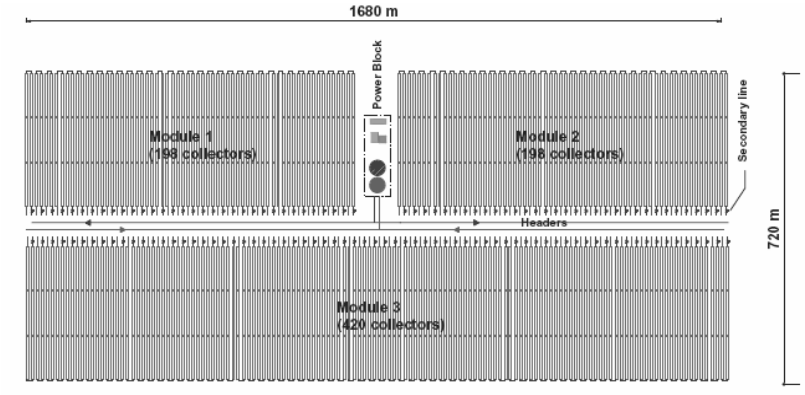

Fig. 3. Layout of the CSP (N-S orientation).

MATLAB based model of the CSP

Unlike a PV plant for which all the three components of solar radiation (direct, diffuse and reflected) are useful for energy production, the CSP utilizes the direct component only. For this aim, it is necessary to know the DNI for the installation site. In this model, we consider that the CSP is located in Bari, a city of the South of Italy different from the installation site of ENEA's project. The values of DNI for Bari are not available, but in Mediterranean countries the values of the DNI are similar to the values of Global Horizontal Irradiation (GHI), as reported in Fig. 4; then, GHI values are used for this paper. As the collectors can rotate on a single axis, it is necessary to define the orientation of their axes, North-South (N-S) or East-West (E-W). Fig 5 reports the values of the average daily radiation for the 12 months of a year (DNI equal to 1731 kWh/m2/year). It can be noted that the radiation on the collector is larger for the N-S orientation than for E-W. Table 2 compares several parameters for both the N-S and E-W orientations, considering a 40MWe rated power CSP. It results that the number of collectors needed, as well as the area of the solar field and the occupied land, is smaller for the N-S orientation than for E-W. Then, the N-S orientation is considered hereafter.

Table I: Parameters of the CSP

Number of collectors	816
Area of each collector	3317.76 m^2
Total collector area	$45*10^4$ m^2
Distance between collectors	11.5 m
Peak power of the solar field (with a radiation of 900W/m^2 and an efficiency of the collector equal to 0.79)	321 MWt
Solar field area	900,000 m^2
Temperature of the hot tank	550 °C
Temperature of the cold tank	290 °C
Storage capacity	3000 MWh
Rated electrical power	40 MWe
Thermo-electrical efficiency in rated electrical power	0.423
Produced energy for year	413 GWh/year
Load factor (ratio between produced energy and energy obtained if the CSP worked in the rated conditions during the whole year)	0.48
Mean collector efficiency for one year (depending on the annual direct radiation)	0.67

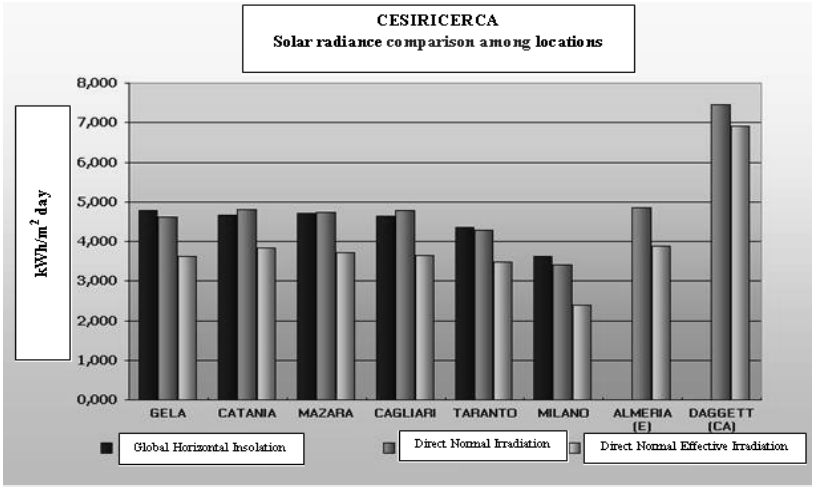

Fig. 4. Comparison between GHI and DNI

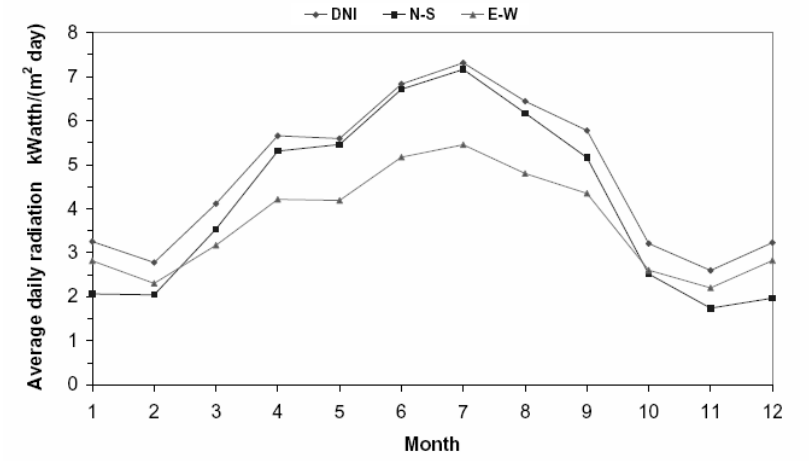

Fig. 5. Solar radiation for the site of Gela (1993, CESI).

Table II: Comparison between N-S and E-W orientations for CSP of 40 MW_e rated power

	N-S	E-W
DNI [kWh/(m^2·year)]	1731	
Radiation on the collector [kWh/(m^2·year)]	1520	1344
Relative radiation (% DNI)	88%	78%
Number of collectors	816	1,008
Area of the solar field [m^2]	451,215	557,384
Occupied land [m^2]	900,000	1,110,000

As the secondary loop and the thermal cycle of Fig. 1 represent the standard operation of a common fossil fuel power station utilizing a Rankine cycle, the model proposed in this paper is limited to the primary loop only, i.e. the thermodynamic system. Fig. 6 reports the proposed algorithm for modelling the primary loop of Fig. 1. It can be noted that two sets of input data are necessary. The former one concerns the installation site: latitude, altitude, climate conditions, available surface, shadings and so on. The latter one is constituted by the geometric dimensions of each collector, number of collectors (depending on the desired electrical power), number of SCAs, typology of fluid, and so on. The first set of input data allows the DNI to be evaluated while the second one allows the layout of the solar field to be defined. Finally, a mathematical model of the thermodynamic system is obtained, considering the fluid starting from the cold tank and arriving to the hot tank, flowing through the network of receivers.

As previously explained, the fluid considered in this paper is constituted by a binary mixture of salts, sodium (60%) and potassium (40%) nitrate. Some physical parameters of this mixture, needed for evaluating the Nusselt number (see later eq. (12)), were obtained by linear regression based on literature data. They are defined in the following equations (T_{salts} is the temperature of the molten salts), while Fig. 7 is a diagrammed representation.

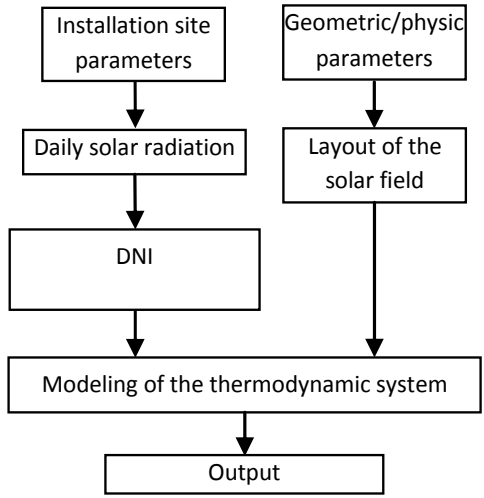

Fig. 6. Modelling steps of primary loop of Fig. 2

- Dynamic viscosity:

$$\mu = \frac{(425,239,400 \cdot T_{salts}^{-2,945})}{1000} \quad (1)$$

- Density:

$$\rho = -0.657 \cdot T_{salts} + 2317.2 \quad (2)$$

- Kinematic viscosity:

$$\nu = \frac{\mu}{\rho} \quad (3)$$

- Specific heat:

$$c_{p_s} = 1443 + 0.172 \cdot (T_{salts} - 273.15) \quad (4)$$

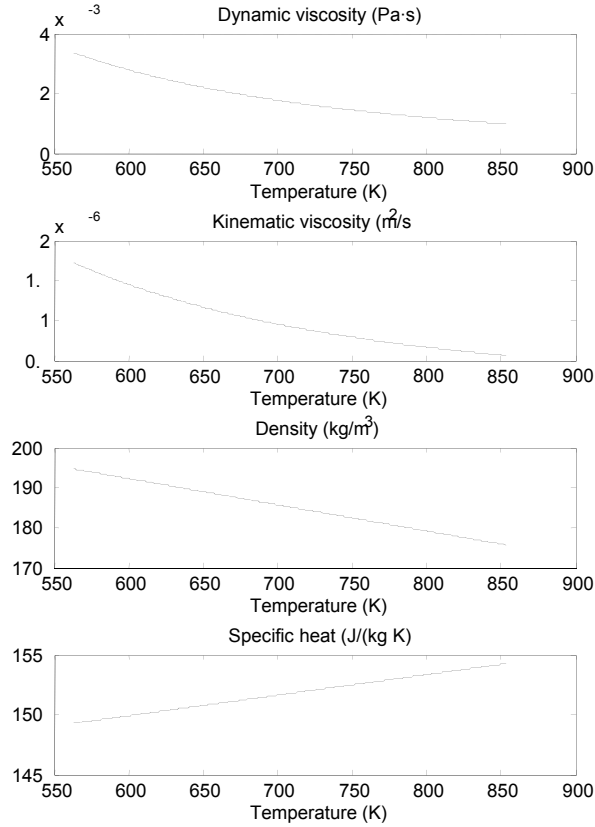

Fig. 7. Some physical parameters of the mixture of salts used for the model.

The output data of the model are the thermal efficiency, the thermal power and the final fluid temperature (corresponding to the fluid stored in the hot tank). As these parameters depend strongly on the thermal losses, it is necessary to evaluate all of them first. In the following, all the considerations will regard a single receiver, also named absorber. Thermal losses of the absorber can be classified as [11]:

1. losses from the receiver to the low-pressure zone inside the glass pipe through radiation, $Q_{ab,r}$, and conduction and convection with the residual gas, $Q_{ab,c}$;

2. losses from the receiver to the external environment due to the metal bellows needed for thermal expansion, Q_b;
3. losses from the glass pipe to the environment due to radiation, $Q_{g,r}$, and to convection, $Q_{g,c}$.

The several contributions can be evaluated as follows [11]:

$$Q_{ab,r} = \frac{\sigma \cdot \left(T_{ab}^4 - T_g^4\right)}{\frac{1}{\varepsilon_{ab}} + \left(\frac{1}{\varepsilon_g} - 1\right) \cdot \frac{r_{ab}}{r_g}} \cdot S_{ab} \tag{5}$$

where σ is the Stefan-Boltzman constant, T_{ab} the absorber temperature, T_g the glass temperature, S_{ab} the surface for the thermal transfer, r_{ab} the radius of the absorber pipe, r_g the radius of the glass pipe, ε_g the emissivity of the glass, and finally ε_{ab} the emissivity of the absorber, depending on the absorber temperature as $\varepsilon_{\text{ab}} = 0.00042 \cdot T_{ab} - 0.0995$;

$$Q_{ab,c} = h_d \cdot \left(T_{ab} - T_g\right) \cdot S_{ab} \tag{6}$$

where h_d is the heat transfer coefficient for the low-density gas [12], depending on the air thermal conductivity, on the mean free path of the particles and on the radiuses of both the absorber and the glass pipe.

$$Q_b \approx 0.15 \cdot Q_{losses} \tag{7}$$

where Q_{losses} represents the total losses.

$$Q_{g,r} = \sigma \cdot \varepsilon_g \cdot \left(T_g^4 - T_{sky}^4\right) \cdot S_g \tag{8}$$

where S_g is the glass surface, while the sky temperature T_{sky} can be evaluated as [14]:

$$T_{sky} = \left(\varepsilon_{sky}\right)^{0.25} \cdot T_a \tag{9}$$

where T_a is the dry bulb temperature, while ε_{sky} is a second-order polynomial function of the dew point ambient temperature.

Finally,

$$Q_{g,c} = h_c \cdot \left(T_g - T_a\right) \cdot S_g \tag{10}$$

where h_c is the external convection heat transfer, equal to:

$$h_c = \frac{\lambda}{2r_g \cdot N_u} \tag{11}$$

where λ is the air thermal conductivity and N_u is the Nusselt number, related to the Reynolds number and to the Prandtl number:

$$Nu = 0.3 + \frac{0.62 \cdot \mathrm{Re}^{0.5} \cdot \mathrm{Pr}^{1/3}}{1 + \left(\frac{0.4}{\mathrm{Pr}}\right)^{2/3}} \cdot \left[1 + \left(\frac{\mathrm{Re}}{282000}\right)^{5/8}\right]^{4/5} \tag{12}$$

Taking into account the previous losses, the thermal efficiency can be calculated as:

$$\eta = \eta_{opt} \cdot k - \frac{Q_{losses}}{I_{direct} \cdot S} \tag{13}$$

where η_{opt} represents the optical efficiency (fixed to 0.8, standard value), S the surface of the collector, I_{direct} the direct radiation and k, taking into account the angle error of the pointing system [14], is defined as:

$$k = \cos\vartheta + 0.000994 \cdot \vartheta - 0.00005369 \cdot \vartheta^2 \tag{14}$$

ϑ being the angle between the incident ray and the normal to the front plane of the reflector.

Finally, the thermal power, Q_{fluid}, can be calculated as:

$$Q_{fluid} = \eta \cdot I_{direct} \cdot l_A \cdot l_s \tag{15}$$

where l_A is the span of the collector and l_s is the length of the SCA.

At this point the final fluid temperature is:

$$T_U = T_I + \frac{Q_{fluid}}{G_s \cdot c_{p_s}} \tag{16}$$

where T_I is the initial temperature (i.e. the fluid temperature in the cold tank), G_s the flow capacity and c_{ps} the specific heat of the molten salts. It can be noted that T_U decreases as G_s increases: in fact, the larger the flow capacity, the shorter the time necessary to pass through the receiver, and the smaller the thermal energy captured by the fluid.

Results

After modelling the thermodynamic system, some simulations were run in Matlab in order to evaluate its performance. To this aim, several input variables were considered because, for example, the thermal performance (i.e. the final temperature of the molten salts, T_U) depends on the length of a single collector, on its flow capacity and on the radiation. Diagrammed output variables, as already said, will be the thermal performance, T_U, the thermal power, Q_{fluid} , and the thermal efficiency, η.

Fig. 8a reports $T_U = f(G_s)$ for several values of radiation. As can be seen, for a fixed value of I_{direct} , T_U decreases as G_s increases, whereas for a fixed value of G_s , T_U increases as I_{direct} increases. Then the correlation between T_U and G_s is opposite with respect to the correlation between T_U and I_{direct} . Fig. 8b resumes the previous considerations in a 3D diagram. Fig. 9 reports the final temperature $T_U = f(l_s)$ for different values of flow capacity G_s . It can be noted that, for $G_s > 3kg/s$, T_U increases linearly as l_s increases, whereas for $G_s \le 3kg/s$ the correlation between TU and l_s is still positive but nonlinear. Fig. 9 was obtained with $I_{direct} = 350\,\mathrm{W/m^2}$; similar diagrams are obtained for different values of I_{direct} .

Fig. 10a diagrams the thermal power depending on the flow capacity of the molten salts, for a fixed value of I_{direct} . In this case, the relation is also linear for higher values of G_s ; otherwise, it is nonlinear. It can be noted that Q_{fluid} increases as G_s increases (for a fixed value of I_{direct}) and as I_{direct} increases (for a fixed value of G_s). Fig. 10b contains all this information in a single 3D diagram.